Steel and Composite Structures, *Vol. 28, No. 1 (2018) 73-82*
DOI: https://doi.org/10.12989/scs.2018.28.1.073

Experimental investigation on shear capacity of partially prefabricated steel reinforced concrete columns

Yong Yang [a], Yang Chen [*], Jintao Zhang [b], Yicong Xue [c], Ruyue Liu [d] and Yunlong Yu [e]

School of Civil Engineering, Xi'an University of Architecture & Technology, Xi'an, Shaanxi 710055, China

(*Received November 8, 2017, Revised April 20, 2018, Accepted April 23, 2018*)

Abstract. This paper experimentally and analytically elucidates the shear behavior and shear bearing capacity of partially prefabricated steel reinforced concrete (PPSRC) columns and hollow partially prefabricated steel reinforced concrete (HPSRC) columns. Seven specimens including five PPSRC column specimens and two HPSRC column specimens were tested under static monotonic loading. In the test, the influences of shear span aspect ratio and difference of cast-in-place concrete strength on the shear behavior of PPSRC and HPSRC columns were investigated. Based on the test results, the failure pattern, the load-displacement behavior and the shear capacity were focused and analyzed. The test results demonstrated that all the column specimens failed in shear failure mode with high bearing capacity and good deformability. Smaller shear span aspect ratio and higher strength of inner concrete resulted in higher shear bearing capacity, with more ductile and better deformability. Furthermore, calculation formula for predicting the ultimate shear capacity of the PPSRC and HPSRC columns were proposed on the basis of the experimental results.

Keywords: prefabricated structure; steel reinforced concrete column; experimental study; shear behavior; shear capacity

1. Introduction

In recent decades, steel reinforced concrete (SRC) columns have been applied in high-rise buildings in the earthquake zone. Owing to the good performance of encased steel section, the SRC columns possess considerable advantages such as high load-carrying capacity, larger stiffness, good fire resistance, as well as easy to delay the local bucking of steel elements (Uy and Bradford 1995, Hajjar 2002, Xue *et al*. 2014, Pereira *et al*. 2016). However, because of the relative complex construction process, the application of SRC columns was not welcomed and widely applied as expected. These years, the use of the precast concrete columns has extensively increased because of the significant saving in labor costs and construction time (Tam *et al*. 2007, Xiao *et al*. 2017). For this reason, precast SRC columns which wholly prefabricated in the shop have been proposed and are introduced to achieve high quality and have been widely in Japan and some countries. But the new problems such as difficult to transport, lift and install because of their larger sectional dimension size and the heavy weight are also presented (Yang *et al*. 2017). Furthermore, the integrity of beam-column joints in entire precast SRC structure is more difficult to guarantee, which always become the biggest problem (Karim *et al*. 2012).

To solve the problem of the entire precast SRC columns, an innovative partially prefabricated steel reinforced concrete (PPSRC) column is proposed in this study (Hwang *et al*. 2016). As shown in Fig. 1, this kind of column is composed of a precast outer-part and a cast-in-place inner-part. The precast outer-part comprises high strength or high performance concrete, steel section, reinforcing bars and stirrups. The outer-part can be prefabricated well in some precast factory or shop. After lifting and installing the precast outer-part on construction site, the normal concrete was cast into the outer part, and then these two parts are well joined together to form a wholly member. To sufficiently ensure the bond on the interface of steel shape and precast concrete as well as inner concrete, a set of high-strength bolt shear connectors are introduced on the steel flange of the steel shape (Yang *et al*. 2016, Agheshlui *et al*. 2017). Therefore, compared with the entire precast SRC columns, in the PPSRC columns, the weight of the precast part was reduced because only the outer part was precast and then the transport problem was solved, and the outer-part and inner-part were better jointed together for the inner concrete was poured on site. Furthermore, compared with SRC columns, several construction procedures such as reinforcement binding and formwork are omitted, which effectively simplify the construction process and reduce the energy consumption of construction.

In PPSRC column, the compressive strength of the concrete in the outer-part could be different from that of the inner-part. It means the prefabricated outer-part could be made of high strength and high performance concrete, while the inner-part can be made of normal strength concrete or lightweight aggregate concrete, and recycled concrete. Therefore, the effect of different materials on the shear behavior of specimens is of great importance.

Shear of SRC column and RC column is a complex phenomenon that is still not very well understood

*Corresponding author, Ph.D. Candidate,
E-mail: xauatchenyang@126.com

ISSN: 1229-9367 (Print), 1598-6233 (Online)

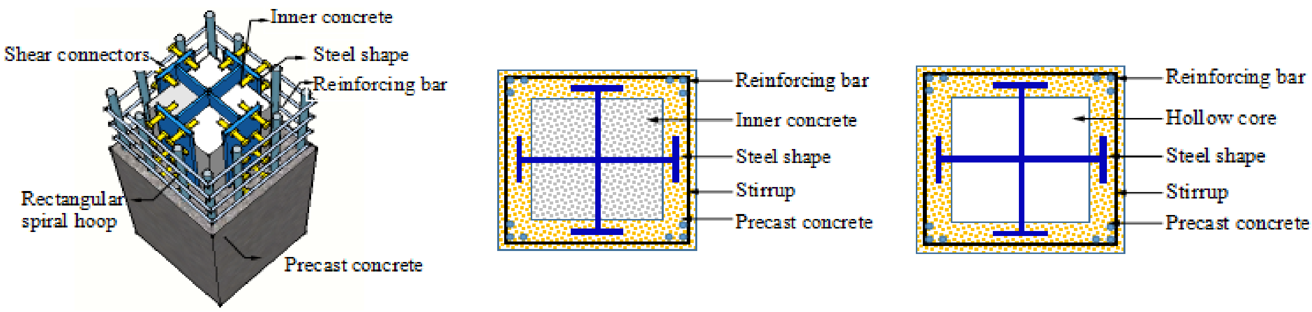

(a) Sketch of PPSRC column (b) Cross-section (c) Hollow-core cross-section

Fig. 1 The schematic diagram of PPSRC column

Table 1 The details of all specimens

Specimen No.	l / mm	h_0 / mm	a / mm	$\lambda = a / h_0$	$f_{cu,out}$ / MPa	$f_{cu,in}$ / MPa	Loading modes
PPSRC-1	1370	320	320	1.0	104.61	21.2	Two points loading
PPSRC-2	1750	320	480	1.5	104.61	21.2	Single point loading
PPSRC-3	2130	320	640	2.0	104.61	21.2	Two points loading
PPSRC-4	1370	320	480	1.5	104.61	44.6	Single point loading
PPSRC-5	1370	320	480	1.5	104.61	104.61	Single point loading
HPSRC-1	1370	320	480	1.5	104.61	0	Two points loading
HPSRC-2	2130	320	640	2.0	104.61	0	Two points loading

*Note: l denotes the length of the column, h_0 denotes the effective depth of section, a denotes the shear span, and λ denotes the shear span aspect ratio and $\lambda = a/h_0$

(Albegmprli *et al*. 2015, Kang *et al*. 2015, Trentadue *et al*. 2015, Vora and Shah 2016). To investigate the shear behavior of this new kind of column, a set of tests on PPSRC and hollow partially prefabricated steel reinforced concrete (HPSRC) columns were conducted. The parameters including the shear span aspect ratio and difference of concrete strength of inner part and outer part were focused and investigated. Based on the test results, a formula for calculating the shear bearing capacity of the PPSRC and HPSRC column was put forward and presented.

2. Test program

2.1 Test specimens

A total of seven composite column specimens were manufactured and tested, including five PPSRC columns and two HPSRC columns. Parameters including the shear span aspect ratio (1.0, 1.5 and 2.0) and the strength of inner concrete (C20, C40 and C90) were considered in the experiment. The tested specimens were classified as PPSRC groups and HPSRC groups. The details of all specimens are tabulated in Table 1.

All the column specimens had a square cross section of size 350×350 mm and were longitudinally reinforced by 8 bars of 32 mm diameter high-grade steel (PSB1080). Hot-rolled plain steel bar with diameter of 8 mm was used for stirrups. Details of specimens section are shown in Fig. 2. The thickness of concrete encasement in all the specimens was 87.5 mm, which was determined by the cover thickness and arrangement of reinforcement. The cross-steel shape section in all specimens was fabricated with two H-shaped steel sections welding together, HN175 mm × 90 mm × 5 mm × 8 mm (dimensions in mm for depth, width, web thickness, and flange thickness, respectively). Four riffled plates and the steel flange were acted as formworks for inner concrete. Furthermore, to ensure the composite action between the precast concrete and the cast-in-place concrete, high strength bolts connectors were interlaced on the steel flange of steel shape, as shown in Fig. 2.

2.2 Material properties

In the experiment, reinforcing bars of 32 mm in diameter and PSB1080 in grade were used as the longitudinal reinforcement, and its average yield strength and ultimate tensile strength were 1103 MPa and 1211 MPa, respectively. B8 bars of 8 mm in diameter and HRB335 in grade were used as the stirrup, and its average yield strength and ultimate tensile strength were 416 MPa and 520 MPa, respectively. Coupons were cut from the flange and web of the rolled steel shape HN175 mm × 90 mm × 5 mm × 8 mm with Q235 grade according to Chinese steel standard (GB/T 700-2006). For the flange of steel shape, the tested yielding strength was 312 MPa and ultimate strength was 418 MPa, respectively, while for the web of steel shape, the tested yielding strength was 273 MPa and ultimate strength was 520 MPa, respectively.

The strength grade of the concrete in the outer-part of PPSRC columns and the inner-part were designed to be different. The strength grade of the precast concrete in

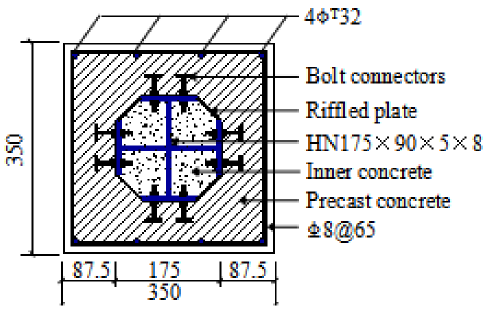

(a) Cross-section of PPSRC columns

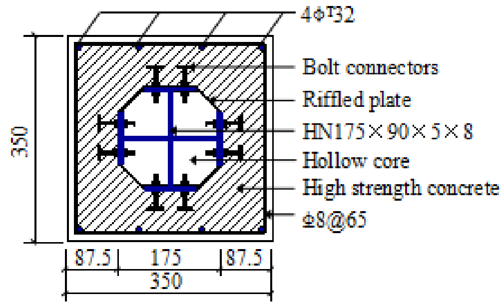

(b) Cross-section of HPSRC columns

Fig. 2 Schematic diagram of column specimens

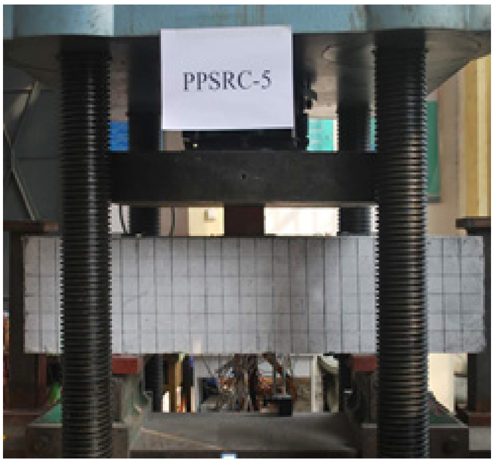

(a) Cross-section of PPSRC columns

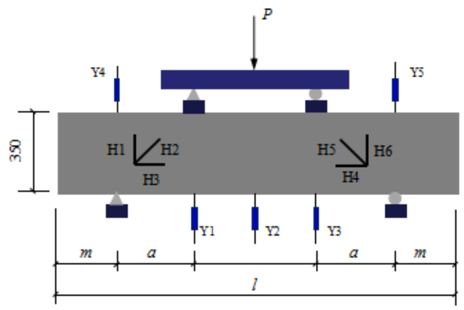

(b) Two points loading

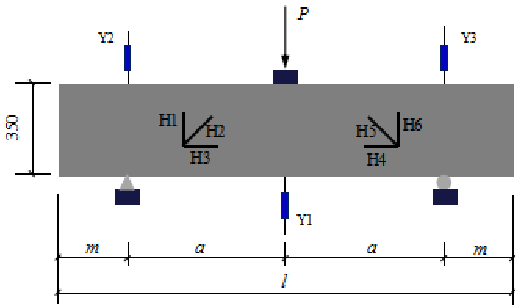

(c) Single point loading

Fig. 3 Diagram and photo of test setup

outer-part was designed as C90, while the inner-part was designed at three levels as C20, C40 and C90. Standard concrete cubes with dimensions of 150 mm × 150 mm × 150 mm were used to determine compressive strength in accordance with the code for design of concrete structures (GB/T 50081-2010), and the average compressive strengths of concrete cubes obtained for different specimens were listed in Table 1.

2.3 Test setup and procedure

The loading equipment and setup for columns specimens are shown in Fig. 3. The loading equipment was an electro hydraulic servo-testing machine with a capacity of 5000 kN. Two loading methods were adopted in the experiment including single point loading at the mid-span of column and two points loading by a distribution beam and two cross beams. The load was applied on the specimens at a constant displacement rate of 0.3 mm/min in a monotonic manner. To ensure uniform pressure distribution, a layer of sand was placed at the surface of loading point of the specimens. During the test, linear variable displacement transducers (LVDTs) were used to monitor and record the displacement of loading point and two supporting beams during the test. Strain gauges were used to measure the strain responses of the web of the steel shape and stirrup. The details of the loading scheme and the layout of LVDTs are presented in Fig. 3, and the layout of the strain gauges is plotted in Fig. 4.

3. Experimental results and discussions

3.1 Observed behavior and failure mode

All the specimens failed in shear and the similar failure modes were observed for HPSRC and PPSRC column specimens. In the experiment, there was no obvious slippage observed at the interface between the precast concrete and the inner concrete, which indicated that the

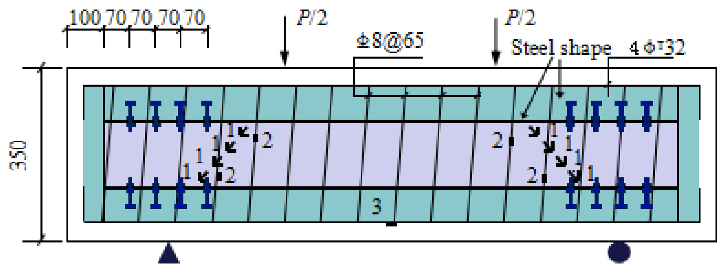

1—Steel web strain gauges 2—Stirrup strain gauges 3—Longitudinal strain gauges

Fig. 4 Layout of strain gauges of specimens

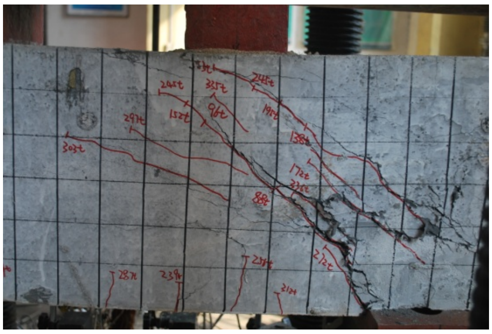

(a) PPSRC-1

(b) PPSRC-4

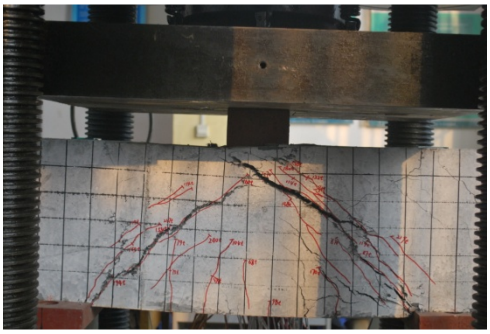

(c) PPSRC-2

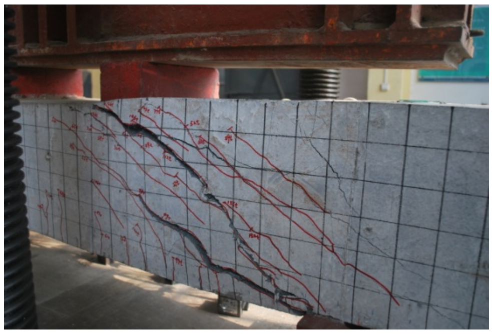

(d) HPSRC-2

Fig. 5 Typical failure modes and damage patterns of specimens

outer-part concrete of PPSRC columns was bonded well with inner cast-in-place concrete. Moreover, the ductile failure modes were achieved due to the contribution of steel shape and were depended on the shear span aspect ratio of the columns. Photos of the crack patterns and the failure modes of the specimens are presented in Fig. 5.

For specimen PPSRC-1, the shear cracks developed prior to flexural cracks, and diagonal shear crack initiated at the shear span of the specimen at approximately $0.2V_u$. Then the new diagonal cracks developed with the load increasing, but the bending cracks developed slowly. When the load reached about $0.8V_u$, the diagonal cracks in critical section occurred, and these cracks expanded gradually as the load increased. Finally, the failure mode was dominated by the crushing of concrete in critical section.

For the other specimens, the flexural cracks initiated at about $0.2V_u$, and then some minor shear diagonal cracks appeared in shear span with loading increasing. Subsequently, the critical diagonal crack formed and gradually stretched to the loading point at about $(0.70\sim0.85)V_u$. Meanwhile, the height of the shear compression zone decreased and the concrete in compression zone failed with a complex stress state. Finally, the diagonal cracks developed and resulted in significant drop of the shear capacity.

3.2 Shear force-displacement curves

Results obtained from the experiment are presented in Table 2, in terms of cracking load V_{cr}, ultimate load V_u, yield displacement δ_y, ultimate displacement δ_u, and the ductility coefficient μ of all specimens. Fig. 6 shows the shear force-displacement curves at the mid-span point of the column specimens. From the shear force-displacement curves, it can be observed that both the ultimate strength and initial stiffness of specimens increased with the decreasing of shear span aspect ratio. The shear behavior of HPSRC columns was similar to that of PPSRC columns, in

Table 2 Test results of specimens

Specimen No.	V_{cr} (kN)	V_u (kN)	Δ_y (mm)	δ_u (mm)	$\mu = \delta_u/\delta_y$
PPSRC-1	442	2055	4.01	12.89	3.21
PPSRC-2	376	1446	5.00	17.28	3.46
PPSRC-3	196	1154	5.07	16.57	3.27
PPSRC-4	412	1525	2.89	8.96	3.10
PPSRC-5	512	1815	5.36	17.56	3.28
HPSRC-1	314	1459	5.62	16.89	3.01
HPSRC-2	136	1124	6.05	19.52	3.23

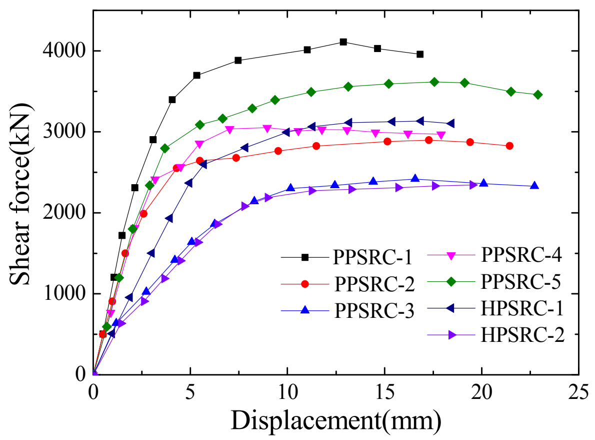

Fig. 6 Shear force-slip curves of specimens

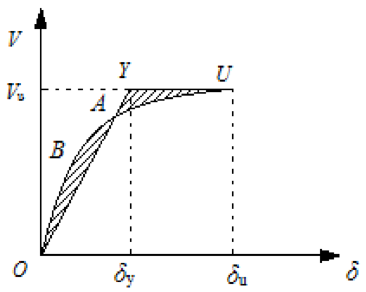

Fig. 7 Definition of yield displacement

which the initial stiffness was just slightly higher. It also can be seen from the curves that the force for all the specimens did not drop significantly after peak load, which indicating both PPSRC and HPSRC columns exhibited highly ductile shear behavior. To evaluate the deformability of the columns, a ductility ratios μ of all specimens defined as the value of ultimate displacement in mid-span of specimens δ_u divided by the yield displacement δ_y was used and the calculation results were tabulated in Table 2, δ_u was the displacement corresponding to the peak load, and δ_y was defined by the energy equivalence method mentioned in reference (Xu *et al.* 2015). As depicted in Fig. 7, to ensure that the area of OAB was equal to that of AYU, the straight line OA was drawn to intersect the shear force-displacement curve at point A, and OA was extended to the intersection (point Y) with a horizontal line corresponding to V_u (point U), then the displacement corresponding to the point Y was the yield displacement δ_y. From the calculated ductility ratio listed in Table 2, the ductility ratios of all the columns including PPSRC columns and HPSRC columns were greater than 3.0. Clearly it is because the steel shape provided not only the shear stress but also the concrete confinement. Consequently, both the PPSRC and HPSRC columns perform outstanding deformability.

3.3 Shear force-strain curve

The relationships between the shear force and the strains of the steel web and stirrup are illustrated in Figs. 8(a)-(b), respectively. It could be seen that the strain developed slowly at the beginning, and this is because the load was mainly carried by the concrete in this stage, and almost no shear force acted on the stirrups and steel web. As the load increasing, the cracks appeared and resulted in the redistribution of the shear stress in cross section, then the shear force was transferred from the concrete to the stirrups and steel webs, which was validated by the rapid increasing strains of stirrups and steel webs. Finally, the strain results of the stirrup and steel web in shear span almost reached yielding strain when the specimen reached its limit. Furthermore, the strains of steel webs were much higher than that of the stirrups at the same load, therefore, it can be

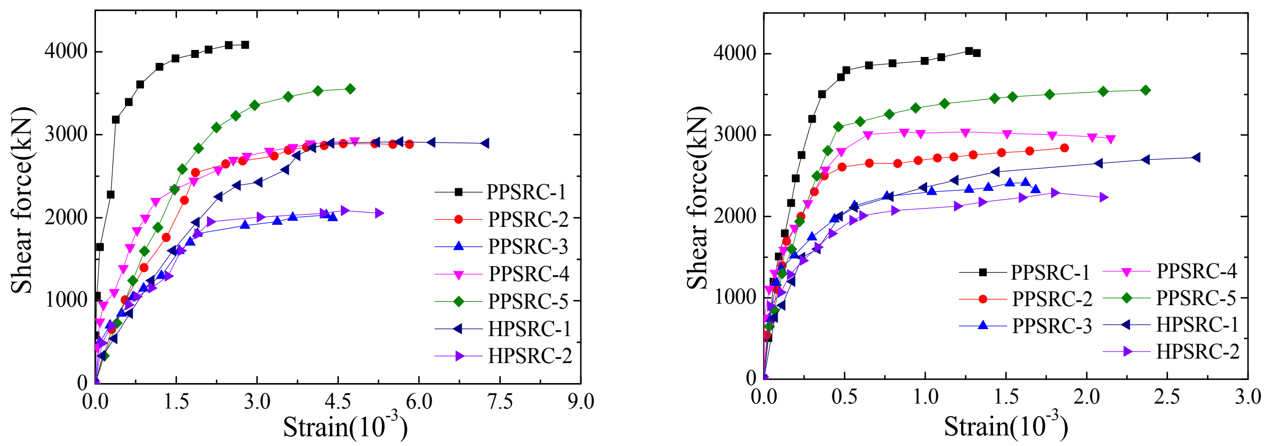

(a) Steel web (b) Stirrup

Fig. 8 Shear force-strain curves of specimens considered that the steel web yielded prior to stirrup and the shear capacity attributed to steel web was greater than that of the stirrups.

4. Analytical work for shear capacity

From the experimental results and the shear force-displacements curves, the results of the shear capacities of the specimens were obtained and listed in Table 2. Some significant factors which have effects on the shear capacity are discussed as follows in this section.

4.1 Effect of cross-section forms

All the specimens were classified into PPSRC groups and HPSRC groups in this study. The ultimate load of specimens PPSRC-3 and HPSRC-2 were 1154 kN and 1124 kN, respectively. As presented in Fig. 9, the shear capacity of specimen PPSRC-3 was approximately 2.7% higher than that of specimen HPSRC-2, which has identical cross-section dimension and shear span aspect ratio with PPSRC-3. Similarly, the shear capacity of specimen HPSRC-1 was 0.9% higher than that of specimens PPSRC-2 but 4.3% lower than specimen PPSRC-4. However, the shear capacity of specimen HPSRC-1 was 19.6% lower than that of specimen PPSRC-5. By comparison, it could be found that the shear capacity of the HPSRC column and the PPSRC column was comparable and was not effected significantly by the cross-section forms when the strength of cast-in-place concrete was less than 44.6 MPa. On the other hand, for long columns, the mechanical behavior of them were dominated by the stability factor, therefore, the stability of HPSRC column and PPSRC column was not much difference because of their comparable stability factor. Moreover, for column with large eccentricity, the mechanical performance of column was dominated by the bending bearing capacity, consequently, it could be concluded that the bending capacity of HPSRC column was almost identical with that of PPSRC column. However, for column with small eccentricity and column subjected to axial loading, the axial capacity of HPSRC column was slightly smaller than that of PPSRC column, therefore, the HPSRC column can be applied to the column with smaller axial compression ratio, such as the column in upper stories.

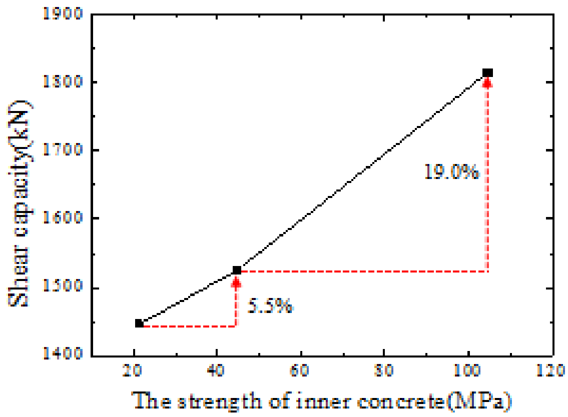

Fig. 10 Shear capacity vs. inner concrete strength curves

4.2 Effect of strength of inner concrete

High-strength concrete was employed as the outer-part of specimens in the experiment, but the strengths of inner concrete were designed to be different. For the specimens PPSRC-2, PPSRC-4 and PPSRC-5, the cross section and the shear span aspect ratio were same, while the strengths of inner concrete were 21.2 MPa, 44.6 MPa, and 104.61 MPa, and the tested ultimate load were 1446 kN, 1525 kN and 1815 kN, respectively. Consequently, it could be concluded that the strength of cast-in-place concrete had a significant influence on the shear capacity of PPSRC columns, and the shear capacity increased proportionally to the increasing of the concrete strength, as shown in Fig. 10.

4.3 Effect of shear span aspect ratio

Fig. 11 showed the relationship of the shear span aspect ratio and the shear capacity of PPSRC and HPSRC column specimens. From Fig. 11, it can be observed that the shear span aspect ratio had a direct effect on the shear capacity of column specimens. For instance, specimens PPSRC-1, PPSRC-2 and PPSRC-3, which were identical in sectional dimension and concrete compressive strength, the shear

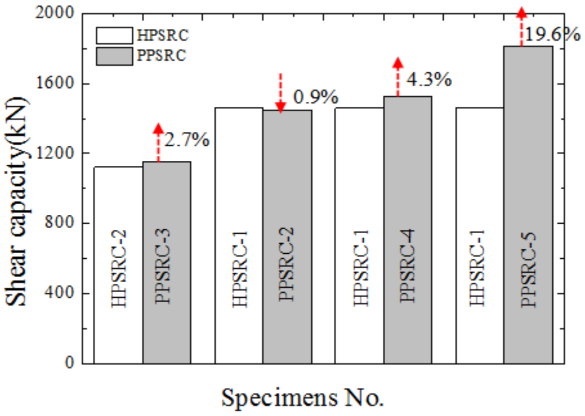

Fig. 9 Comparisons on shear capacities

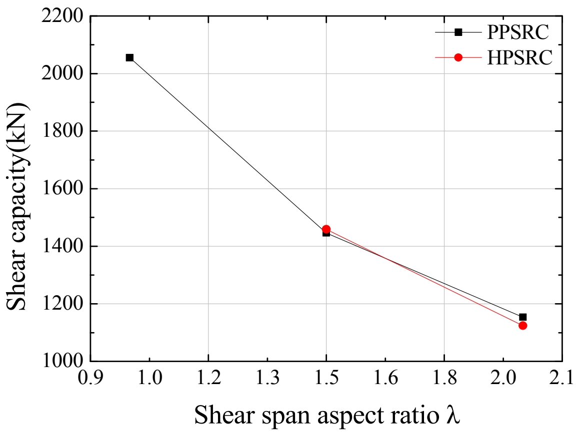

Fig. 11 Shear capacity vs. shear span aspect ratio curves

span aspect ratio were 1.0, 1.5 and 2.0 respectively and the corresponding shear capacities of them were 2055 kN, 1446 kN, and 1154 kN, respectively. In addition, the developments of shear capacity for specimen HPSRC-1 and specimen HPSRC-2 were similar with PPSRC columns. It is evident that the shear capacities of PPSRC columns and HPSRC columns decrease as the shear span aspect ratios increase.

5. Calculation of shear capacity

A calculation formula for the shear capacity of composite columns was proposed on the basis of the experiment and analyses. The proposed equation was expressed by adding the shear capacity of the steel shape to the shear capacity of reinforced concrete

$$V_u = V_a + V_{rc} \tag{1}$$

Where: V_u is the ultimate strength of the specimens; V_a is the shear capacity of the steel web, and V_{rc} is the shear capacity of reinforced concrete.

5.1 Shear capacity of steel shape

As mentioned in literature (Zhao 2001), the bending moment of column is mainly carried by the steel flange, while the shear force and the compression force are carried by the steel web. To evaluate the shear capacity of steel web, it is assumed that the steel web is in a pure shear state, and the effect of shear span aspect ratio is also considered. Therefore, the shear capacity of the steel web can be determined by the following formula

$$V_a = \frac{f_a}{\lambda\sqrt{3}} t_w h_w \tag{2}$$

Where, t_w, h_w and f_a are the thickness, the height and the yielding strength of steel web, respectively.

5.2 Shear capacity of reinforced concrete

As with AIJ design equations, the truss-arch model was adopted to calculate the shear capacity of reinforced concrete (AIJ 1998). This approach suggested that the shear force carried by the transverse reinforcement due to the truss action and diagonal concrete struts due to the arch action should be taken into consideration when calculating the shear strength of the reinforced concrete (Safa *et al.* 2016), thus

$$V_{rc} = V_{tu} + V_{cu} \tag{3}$$

where, V_{tu} is the shear bearing capacity of transverse reinforcement, V_{cu} is the shear bearing capacity of concrete.

(1) Truss model

In the truss model, the shear capacity is composed of the contributions of stirrup, the longitudinal bar and the concrete. The longitudinal reinforcement is considered as

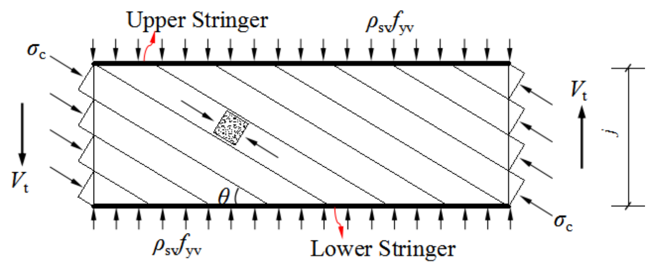

Fig. 12 Truss model

stringer, the stirrup is considered as vertical tensile bar, then the concrete on diagonal section is considered as an inclined compression chord. Fig. 12 shows the mechanism details for the truss model and the vertical component of inclined compression chord is given by

$$V_c = \sigma_c b_e j \cos\theta \sin\theta \tag{4}$$

Where, b_e is the effective width of the cross-section, θ is the inclined crack angle with respect to the longitudinal axis of column, and j is the distance between upper and lower chords of the analogous truss.

When the stirrups yield, the shear force V_{tu} carried by the transverse reinforcement is given by

$$V_{tu} = \rho_{sv} f_{yv} b_e j \cos\varphi_1 \cot\theta \tag{5}$$

Where ρ_{sv} is the ratio of transverse reinforcement, f_{yv} is the yield strength of transverse reinforcement. Considering that the angle φ_1 between stirrup and vertical directions was extremely small and the value of $\cos\varphi_1$ could be taken as 1.0, therefore the Eq. (5) can be converted as following

$$V_{tu} = \rho_{sv} f_{yv} b_e j \cot\theta \tag{6}$$

Finally, the corresponding compression stress on the concrete can be determined combining with Eqs. (4) and (6)

$$\sigma_c = \frac{\rho_{sv} f_{yv} \cot\theta}{\cos\theta \sin\theta} = \rho_{sv} f_{yv} (1 + \cot^2\theta) \tag{7}$$

For the truss model, the inclined crack angle θ has been defined in various specifications, and its value varies from 26.6° to 45° according to the CEB-FIP Model Code. Priestley suggested that the angle θ should be taken as 30° (Priestley *et al.* 1994). In Chinese code (GB50010-2010), θ = 45° was usually adopted to calculate the shear force carried by the stirrups according to the truss model. Furthermore, θ = 45° was also recommended by ACI design approach (ACI318 2011), which is the basis for most of reinforced concrete design in US. Therefore, θ equaling to 45° was also preferred in truss model in accordance with the recommendation above.

(2) Arch model

In truss model analysis, the optimal failure mode is that when the stirrups yield, the concrete also reached

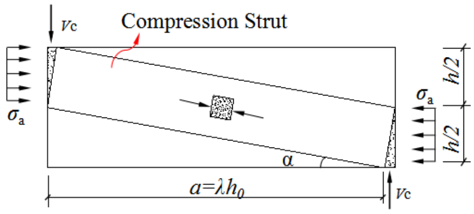

Fig. 13 Arch model

compressive strength f_{ck} (Pan and Li 2013). It means the concrete and the stirrups achieve the maximum load synchronously. But in reality, when the stirrup yields, the strength of concrete σ_c is still less than the compressive strength f_{ck}, here the strength of concrete in arch model between them could be expressed as $\sigma_a = f_{ck} - \sigma_c$.

The load transfer mechanism of the concrete in arch model is shown in Fig. 13. It can be seen that the compression strut subjected to tensile stress is perpendicular to the compression direction, and the concrete strength could be reduced to γf_{ck} compared to uniaxial compression state (Collins and Mitchel 1986), where γ denotes the softening coefficient of concrete. Therefore, the diagonal compression stress of the concrete in the arch model can be expressed as $\sigma_a = \gamma f_{ck} - \sigma_c$. However, few reliable methods are available to be used to estimate the value of softening coefficient γ. It was suggested that the softening coefficient could be taken as $\gamma = 0.7 - f_c/200$ (Nielsen 2011). Furthermore, It was considered that the diagonal compression stress was nonlinear with the strength of concrete, and $\gamma = 4.1 f_c^{-0.53}$ was proposed on the basis of experimental results and theoretical analysis (Chen and Nielsen 1988). In this paper, a constant value of γ was determined as 0.6 according to ACI design method and the relationship between the cylindrical compressive strength and the prismatic compressive strength (Zhang *et al.* 2014).

The shear force V_c carried by arch action is based on an assumption that the compression zone depth is half of the member depth, as shown in Fig. 13, and thus

$$V_c = \sigma_a \frac{bh}{2} \tan\alpha \tag{8}$$

Where α is varied based on the accurate condition shown in Fig. 14. Considering the confinement effects contributed from the steel shape, the concrete in the cross section of the column specimens is divided into three parts and its shear transfer mechanism in arch model can be simplified as shown in Figs. 14 (a)-(c).

In arch model, the shear capacity of the concrete on the left and right of the flange can be determined by

$$V_1 = \sigma_a \frac{(b - h_w - 2t_f)h}{2} \tan\alpha_1 \tag{9}$$

Similarly, the shear capacity of the concrete inside the steel flange can be calculated by

$$V_2 = \sigma_a \frac{(h_w + 2t_f - t_w)^2}{2} \tan\alpha_2 \tag{10}$$

Considering the confinement effects contributed from the steel shape (Chen and Lin 2006, Wang *et al.* 2016, Chen and Wu 2017), the softening coefficient of the concrete γ was determined as = 1.0 in Eq. (10).

The shear capacity of concrete on the upper and lower sides of the steel flange can be expressed as following

$$V_3 = \sigma_a \frac{(h_w + 2t_f)[h - (h_w + 2t_f)]}{2} \tan\alpha_3 \tag{11}$$

Therefore, the contribution of concrete to the shear capacity of PPSRC column can be obtained by superimposing the shear capacity of these three parts

$$V_{cu} = V_1 + V_2 + V_3 \tag{12}$$

Then, the shear capacity of PPSRC column can be estimated by Eq. (13)

$$\begin{aligned} V_u &= V_a + V_{rc} = V_a + V_{tu} + V_{cu} \\ &= \frac{f_a}{\lambda\sqrt{3}} t_w h_w + \rho_{sv} f_{yv} b_e j \\ &+ \frac{1}{2}(f_{ck} - 2\rho_{sv} f_{yv})(h_w + 2t_f - t_w)^2 \tan\alpha_2 \end{aligned} \tag{13}$$

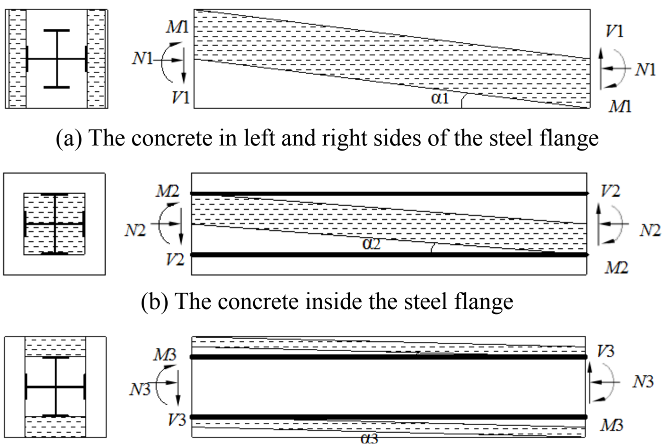

(a) The concrete in left and right sides of the steel flange

(b) The concrete inside the steel flange

(c) The concrete in upper and lower sides of the steel flange

Fig. 14 Arch model in PPSRC column specimen

Table 3 Comparison of test results and calculated results

Specimen No.	V_u (kN)	V_{c1} (kN)	V_{c2} (kN)	V_{up} (kN)	V_{c1}/V_u	V_{c2}/V_u	V_{up}/V_u
PPSRC-1	2055	925	1029	1712	0.45	0.50	0.83
PPSRC-2	1446	762	914	1258	0.53	0.63	0.87
PPSRC-3	1154	661	838	1031	0.57	0.73	0.89
PPSRC-4	1525	777	929	1322	0.51	0.61	0.87
PPSRC-5	1815	806	958	1488	0.44	0.53	0.82
HPSRC-1	1459	732	884	1210	0.50	0.61	0.83
HPSRC-2	1124	636	812	995	0.57	0.72	0.89
Average ratio of measured to calculated value					0.51	0.62	0.86
Coefficient of variation					0.08	0.11	0.03

*Note: V_u is the tested shear capacity, V_{c1} is the shear capacity obtained by JGJ method, V_{c2} is the shear capacity obtained by AIJ method, V_{up} is the shear capacity obtained by proposed method

$$+\frac{1}{2}(\gamma f_{ck}-2\rho_{\mathrm{sv}}f_{\mathrm{yv}})[(b-h_{\mathrm{w}}-2t_{\mathrm{f}})h\tan\alpha_1 + (h_{\mathrm{w}}+2t_{\mathrm{f}})(h-h_{\mathrm{w}}-2t_{\mathrm{f}})\tan\alpha_3] \quad (13)$$

Where

$$\tan\alpha_1=\frac{h}{2\lambda h_0},\ \tan\alpha_2=\frac{h_{\mathrm{w}}+2t_{\mathrm{f}}}{2\lambda h_0},$$

$$\tan\alpha_3=\frac{h-h_{\mathrm{w}}-2t_{\mathrm{f}}}{2\lambda h_0}.$$

Finally, the shear bearing capacity of PPSRC column can be obtained by Eq. (13). It should be noted that the shear capacity of the concrete inside the steel flange should be eliminated when calculating the shear bearing capacity of HPSRC column. In Table 3, the shear capacities predicted by the proposed method, V_{up}, are compared with the experimental results, V_u, in terms of different specimens, and the average value of the ratios of the strengths predicted by the proposed method to the test results is 0.86 and the corresponding coefficient of variation is 0.03. Meanwhile, the results from Chinese specification (JGJ138-2016) and Japanese specification AIJ are also calculated and compared with experimental results, the final results are also listed in Table 3. It can be found that both existed methods excessively underestimate the shear capacities of all specimens. Compared with the shear capacities calculated by JGJ138-2016 and AIJ methods, the strengths obtained by the proposed method match well with the experimental results, with smaller and allowable deviation. These results show that the proposed method provides a reliable method for predicting the shear capacity of PPSRC and HPSRC column.

6. Conclusions

This paper provides the experimental and analytical results of PPSRC and HPSRC columns subjected to static monotonic loading. Seven column specimens were tested to investigate the shear behavior of PPSRC and HPSRC columns. Besides, Parametric study including the effect of shear span aspect ratio and the strength of cast-in-place concrete was performed based on the experimental and analytical study, some valuable conclusions could be drawn as following:

- In the experiment, there was no obvious slippage observed at the interface between the precast concrete and the inner concrete, which indicated that the expected composite action was achieved and the type of cross-section proposed in this paper is feasible.
- The shear behavior of the PPSRC column specimens is similar to that of the HPSRC column specimens. All of the specimens developed expected shear failure mode, and the failure mode was ductile because of the steel shape.
- Both the PPSRC column and HPSRC column specimens demonstrated a high shear capacity, and the shear capacity would increase with the decreasing of shear span aspect ratio and with the increasing of the strength of cast-in-place concrete. However, the bearing capacity of HPSRC column specimens is comparable that of PPSRC column specimens with identical dimension when the shear span aspect ratio ranges from 1.5 to 2.0 and the design strength of inner concrete is below C40.
- Equations for predicting the shear capacities of PPSRC column and HPSRC column were put forward on the basis of truss-arch model. Meanwhile, results calculated by proposed approach were compared with experimental results. In addition, calculated results from AIJ and JGJ were compared with tested results to better demonstrate the reliability of proposed method. Consequently, the comparisons indicate that the proposed method could provide more reliable prediction of shear bearing capacity of PPSRC and HPSRC columns than AIJ and JGJ methods.

Acknowledgments

The experiments were sponsored by the National Natural Science Foundation of China (Program No. 51578443 and No. 51778525), National Research and Development Program of China (Program No.

2016YFC0701400) and also supported by the Program for Changjiang Scholars as well as the Program for Innovative Research Team of Xi'an University of Architecture and Technology.

References

ACI318 (2011), Building code requirements for structural concrete and commentary; American Concrete Institute; Farmington Hill, MI, USA.

Agheshlui, H., Goldsworthy, H., Gad, E. and Mirza, O. (2017), "Anchored blind bolted composite connection to a concrete filled steel tubular column", *Steel Compos. Struct., Int. J.*, **23**(1), 115-130.

AIJ (1998), Calculation standard and explication of steel reinforced concrete structures; Architectural Institute of Japan, Atomic Energy Press. [Translated by N.Q. Feng, L.P. Ye, in Chinese]

Albegmprli, H.M.A., Cevik, A., Gulsan, M.E. and Kurtoglu, A.E. (2015), "Reliability analysis of reinforced concrete haunched beams shear capacity based on stochastic nonlinear fe analysis", *Comput. Concrete, Int. J.*, **15**(2), 259-277.

Chen, C.C. and Lin, N.J. (2006), "Analytical model for predicting axial capacity and behavior of concrete encased steel composite stub columns", *J. Constr. Steel Res.*, **62**(5), 424-433.

Chen, G.W. and Nielsen, M.P. (1988), Plastic analysis of shear in beams, deep beams and corbels, Technical University of Denmark (DTU), BYG-Rapport; No. R-237, Kongens Lyngby, Denmark.

Chen, S. and Wu, P. (2017), "Analytical model for predicting axial compressive behavior of steel reinforced concrete column", *J. Constr. Steel Res.*, **128**, 649-660.

Collins, M.P. and Mitchell, D. (1986), "Rational approach to shear design-the 1984 Canadian code provisions", *J. Neurosci. Official J. Soc. Neurosci.*, **83**(6), 925-933.

GB/T 700-2006 (2006), Carbon structure steels; China Planning Press, Beijing, China.

GB/T 50081-2010 (2010), Standard for test method of mechanical properties on ordinary concrete; China Planning Press, Beijing, China.

GB/T 50010-2010 (2010), Code for design of concrete structures; China Architecture and Building Press, Beijing, China.

Hajjar, J.F. (2002), "Composite steel and concrete structural systems for seismic engineering", *J. Constr. Steel Res.*, **58**(5), 703-723.

Hwang, J.H., Lee, D.H., Oh, J.Y., Choi, S.H., Kang, S.K. and Seo, S.Y. (2016), "Seismic performances of centrifugally-formed hollow-core precast columns with multi-interlocking spirals", *Steel Compos. Struct., Int. J.*, **20**(6), 1259-1274.

Jaillon, L. and Poon, C.S. (2010), "Design issues of using prefabrication in Hong Kong building construction", *Construct. Manag. Econ.*, **28**(10), 1025-1042.

JGJ138 (2016), Code for design of composite structures; China Building Industry Press, Beijing, China.

Kang, L., Leon, R.T. and Lu, X. (2015), "Shear strength analyses of internal diaphragm connections to CFT columns", *Steel Compos. Struct., Int. J.*, **18**(5), 1083-1101.

Karimi, K., El-Dakhakhni, W.W. and Tait, M.J. (2012), "Behavior of slender steel-concrete composite columns wrapped with FRP jackets", *J. Perform. Constr. Facil.*, **26**(5), 590-599.

Nielsen, M.P. (2011), *Limit Analysis and Concrete Plasticity*, Rnford Onr.

Pan, Z.F. and Li, B. (2013), "Truss-arch model for shear strength of shear-critical reinforced concrete columns", *J. Struct. Eng.*, **139**(4), 548-560.

Pereira, M.F., Nardin, S.D. and Debs, A.L.H.C.E. (2016), "Structural behavior of partially encased composite columns under axial loads", *Steel Compos. Struct., Int. J.*, **20**(6), 1305-1322.

Priestley, M.J.N., Verma, R. and Xiao, Y. (1994), "Seismic shear strength of reinforced concrete columns", *J. Struct. Eng.*, **120**(8), 2310-2329.

Safa, M., Shariati, M., Ibrahim, Z., Toghroli, A., Baharom, S.B., Nor, N.M. and Petkovic, D. (2016), "Potential of adaptive neuro fuzzy inference system for evaluating the factors affecting steel-concrete composite beam's shear strength", *Steel Compos. Struct., Int. J.*, **21**(3), 679-688.

Tam, V.W.Y., Tam, C.M., Zeng, S.X. and Ng, W.C.Y. (2007), "Towards adoption of prefabrication in construction", *Build. Environ.*, **42**(10), 3642-3654.

Trentadue, F., Quaranta, G., Greco, R. and Marano, G.C. (2015), "New analytical model for the hoop contribution to the shear capacity of circular reinforced concrete columns", *Comput. Concrete*, **14**(1), 59-71.

Uy, B. and Bradford, M.A. (1995), "Ductility of profiled composite beams. part I: experimental study", *J. Struct. Eng.*, **121**(5), 876-882.

Vora, T.P. and Shah, B.J. (2016), "Experimental investigation on shear capacity of RC beams with GFRP rebar & stirrups", *Steel Compos. Struct., Int. J.*, **21**(6), 1265-1285.

Wang, Q., Shi, Q. and Tian, H. (2016), "Experimental study on shear capacity of src joints with different arrangement and sizes of cross-shaped steel in column", *Steel Compos. Struct., Int. J.*, **21**(2), 267-287.

Xiao, C., Deng, F., Chen, T. and Zhao, Z. (2017), "Experimental study on concrete-encased composite columns with separate steel sections", *Steel Compos. Struct., Int. J.*, **23**(4), 483-491.

Xu, C.H., Zeng, L., Zhou, Q., Tu, X. and Wu, Y. (2015), "Cyclic performance of concrete-encased composite columns with t-shaped steel sections", *Int. J. Civil Eng.*, **13**(4), 456-467.

Xue, J.Y., Gao, L., Liu, Z.Q., Zhao, H.T. and Chen, Z.P. (2014), "Experimental study on mechanical performances of lattice steel reinforced concrete inner frame with irregular section columns", *Steel Compos. Struct., Int. J.*, **16**(3), 253-267.

Yang, Y., Yu, Y., Guo, Y., Roeder, C.W., Xue, Y. and Shao, Y. (2016), "Experimental study on shear performance of partially precast castellated steel reinforced concrete (CPSRC) beams", *Steel Compos. Struct., Int. J.*, **21**(2), 289-302.

Yang, Y., Xue, Y., Yu, Y., Ma, N. and Shao, Y. (2017), "Experimental study on flexural performance of partially precast steel reinforced concrete beams", *J. Constr. Steel Res.*, **133**, 192-201.

Zhao, H.T. (2001), *Steel-Concrete Composite Structure*, Science Press, Beijing, China.

Zhang, S.Q., Chen Z.P., Wang, N. and Chen, Y.L. (2014), "Shear mechanism and shear strength of steel reinforced concrete (SRC) cross-shape 3D column-beam joints", *China Civil Eng. J.*, **9**(9), 84-93.

BU